Classical and quantum machine learning applications in spintronics

Kumar J. B. Ghosh*

E.ON Digital Technology GmbH, 45131, Essen, Germany.

Sumit Ghosh†

Institute of Advance Simulations, Forschungszentrum Jülich GmbH, 52428 Jülich, Germany and
Institute of Physics, Johannes Gutenberg-University Mainz, 55128 Mainz, Germany

In this article we demonstrate the applications of classical and quantum machine learning in quantum transport and spintronics. With the help of a two terminal device with magnetic impurity we show how machine learning algorithms can predict the highly non-linear nature of conductance as well as the non-equilibrium spin response function for any random magnetic configuration. We finally describe the applicability of quantum machine learning which has the capability to handle a significantly large configuration space. Our approach is also applicable for molecular systems. These outcomes are crucial in predicting the behaviour of large scale systems where a quantum mechanical calculation is computationally challenging and therefore would play a crucial role in designing nano devices.

I. INTRODUCTION

In the past decade two research areas, namely, artificial intelligence [1] and quantum computation [2], have been a center of attention for their enormous success in solving problems which seems impossible with conventional approach. Fuelled by increasing computer power and algorithmic advances, AI and machine learning techniques have become powerful tools in various research fields, for e.g., material science and chemistry [3–5], power and energy sector [6, 7], cyber security and anomaly detection[8, 9], drug discovery [10], etc. On the other hand, quantum computing has entered a new stage of development in recent years, as fundamental breakthroughs and public interest increased the availability of noisy intermediate-scale quantum (NISQ) devices [11]. There are extensive ongoing efforts on the application of quantum computing in the areas of machine learning [12–14], finance [15], quantum chemistry [16, 17], drug design and molecular modeling [18], power systems [19, 20], metrology [21], to name a few applications. Quantum-enabled methods are the next natural step of the AI studies to support faster computation and more accurate decision making, creating the interdisciplinary field of quantum artificial intelligence [22].

Recently machine learning (ML) and quantum computing (QC) applications are gaining attention in the field of condensed matter physics [23–26]. Most of the studies so far are focused on the electronic properties [27–29] or transport properties [30, 31]. The application of ML has significantly reduced the computational requirement as well as time consumption for computationally demanding problems. In this paper we addressed another very active and promising brunch of condensed matter physics - namely *spintronics* which is focused on

manipulating spin spin degree of freedom and has been in the heart of modern computational device technology. Here we employ classical and quantum machine learning algorithm to predict non-equilibrium spin density generated by an applied electric field as well as the transmission coefficient which are two main observables in spintronics, in a two terminal device configuration in presence of magnetic impurity. This configuration is the basis of any magnetic memory device where the non-equilibrium spin density provides the torque necessary for manipulating the the magnetisation [32, 33]. The theoretical evaluation of non-equilibrium spin density is done via non-equilibrium Green's function technique [34–36] which is computationally computationally quite demanding. Compared to that, prediction with trained learning algorithm is quite efficient [30, 31] and allows to study a large number of configuration for a given system. For a given system, the spintronic properties are usually dominated by a subset of parameters necessary to define the whole system. In ML approach this limited parameters are used to construct the feature space which reduces the dimensionality of the problem significantly. In our case we chose the magnetisation configuration and the transport energy as the governing parameters. For a given arbitrary distribution of magnetisation, the spin response functions as well as the transmission coefficient can be a highly non-linear function of the transport energy. For such high level of non-linearity, conventional regression methods fails to provide reliable outcome over a broad energy range. In this paper we present a new approach to handle this problem. By discretise the continuous outcome, we convert the non-linear regression into a classification problem, we showed that one can have a high level of accuracy with a classical machine learning algorithm. We systematically analysed the transmission and the spin response function over a large range of transport energy and internal parameter. Finally we also demonstrate the applicability of quantum machine learning algorithm which can be useful for exponentially large configuration that is beyond the scope of any classical

---

* jb.ghosh@outlook.com
† s.ghosh@fz-juelich.de

algorithm.

The organisation of this paper is as follows. After a brief introduction in Sec. I, we define our model and methods in Sec. II. It contains the non-equilibrium Green's function method used to generate the training data as well as the classical and quantum ML approach along with our discretisation scheme used to analyse the data. The results and discussions are given in Sec. III, which contains the outcomes of both classical and quantum ML. Finally, in Sec. IV, we offer some concluding remarks.

II. MODEL AND METHOD

A. Tight binding model and non-equilibrium Green's function approach

In this study, we use a two terminal device configuration where a scattering region with magnetic impurity is attached to two semi-infinite non-magnetic electrodes. Here we use only out of plane magnetisation, however this formalism is also applicable for the non-collinear magnetisation as well. The system is defined with a tight binding Hamiltonian

$$H = \sum_{i,\mu\nu} c_{i,\mu}^{\dagger} \epsilon_i^{\mu\nu} c_{i,\nu} + \sum_{\langle ij \rangle, \mu\nu} c_{i,\mu}^{\dagger} t_{ij}^{\mu\nu} c_{j,\nu} \qquad (1)$$

where $\epsilon_i^{\mu\nu}$ is the onsite potential and $t_{ij}^{\mu\nu}$ is the nearest neighbour hopping term. Here we consider Rashba-Bychkov type hopping for the spin dependent part which can be realised on the surface of a heavy metal such as Pt or W and can be induced to other material with proximity effect. The full hopping term along $\hat{x}$ and $\hat{y}$ direction is given by $t_{\boldsymbol{r}+\hat{x}}=t_0\mathbb{I}_2-it_R\sigma_y$ and $t_{\boldsymbol{r}+\hat{y}}=t_0\mathbb{I}_2+it_R\sigma_x$, where $\mathbb{I}_2$ is the identity matrix of rank 2 and $\sigma_{x,y,z}$ are the Pauli matrices. t_0 is the spin independent hopping amplitude and t_R is Rashba coefficient. The onsite energies are also consist of both magnetic and nonmagnetic parts and is given by $\epsilon_i=4|t_0|\mathbb{I}_2+m_i\Delta\sigma_z$ where $m_i=0,\pm1$ corresponding to non-magnetic sites, sites with positive and negative magnetisation respectively, and Δ is the exchange energy. We choose the exchange splitting Δ as the unit of our energy and choose t_0=-0.5Δ. Unless otherwise mentioned t_R is kept at 0.1Δ. We consider a 12×12 scattering region with uniformly spaced 16 magnetic centres (Fig.1) where the magnetisation directions are being chosen randomly. The electrodes are chosen to be non-magnetic with same hopping parameters

The conductance of the system is calculated using Green's function. For simplicity we adopt natural unit here (c=e=$\hbar$=1). The transmission probability and therefore the conductance from left to right electrode is given by $T = Tr\left[\Gamma_1 G^R \Gamma_2 G^A\right]$, where $G^{R,A}$=$[E$-H_S-$\Sigma_1^{R,A}$-$\Sigma_2^{R,A}]^{-1}$ is the retarded/advanced Green's function of the scattering region. $\Gamma_{1,2} = i\left[\Sigma_{1,2}^R - \Sigma_{1,2}^A\right]$, where $\Sigma_{1,2}^{R,A}$ is the retarded/advanced self energy of the
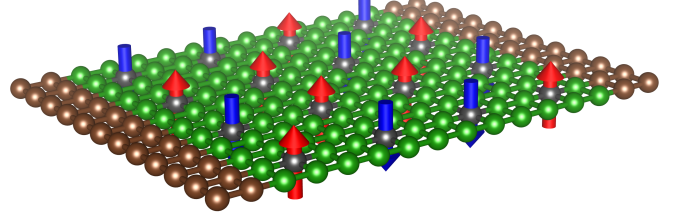

FIG. 1. Schematic of a two terminal device. Green region shows the scattering region. The green sites show the non-magnetic sites and gray sites show magnetic sites with up (red) and down (blue) magnetisation.

left/right electrode. To calculate the the non-equilibrium spin densities one can utilise the lesser Green's function [37, 38] defined as $G^<(E)= G^R(E)\Sigma^<(E)G^A(E)$, where $\Sigma^<(E)=i[f_1(E)\Gamma_1(E)+f_2(E)\Gamma_2(E)]$, with $f(E)$ being the Fermi-Dirac distribution of the corresponding electrode. The non-equilibrium expectation value of a an observable $\mathcal{O}$ at energy E subjected to a bias voltage V is given by

$$\langle\hat{O}\rangle_E = \int_{E-V/2}^{E+V/2} d\epsilon \, Tr\left[\hat{\mathcal{O}} \cdot \rho(\epsilon)\right], \qquad (2)$$

where $\rho(E)=\frac{1}{2\pi i}G^<(E)$ is the non-equilibrium density matrix. For an infinitesimal bias voltage ($V \rightarrow 0$) it is convenient to calculate the response function. Here we are interested in the response function for the in-plane spin component given by $S_i^{x,y}=Tr[\sigma_{x,y} \cdot \rho_i]$, where ρ_i being the projection of the density matrix on ith site. For our calculation we use the tight-binding software KWANT [39] where the non-equilibrium density matrix can be obtained via the scattering wave-function. We generate the conductance and in-plane spin response for randomly chosen spin configurations and energies and use them to train our algorithm.

B. Non-linearity of the response

Let us first consider the intrinsic nature of the system under consideration and the inherent non-linearity of its conductance and spin response function. We start by looking at the band structures of the non-magnetic electrodes for different values of t_R (Fig. 2).

For a clean and homogeneous system, the transmission probability and therefore the conductance shows a step like behaviour. In presence of the magnetic sites in the scattering region this behaviour becomes highly non linear. For this study we focus on three different entities, namely the conductance and the x and y component of the spin response on the magnetic sites (Fig. 3).

One can readily see from Fig.3 that the responses are highly nonlinear in nature within our chosen energy window and completely uncorrelated for different magnetic
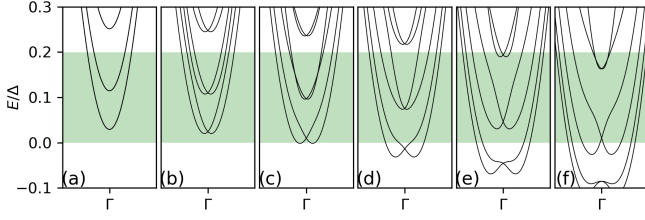
FIG. 2. Variation of lead band structure with t_R. (a), (b), (c), (d), (e), and (f) show the band structures for $t_R=0.00\Delta$, 0.05Δ, 0.10Δ, 0.15Δ, 0.20Δ, and 0.25Δ respectively. The horizontal dashed line show the zero energy level and gray region denotes the energy window where the analysis has been done.
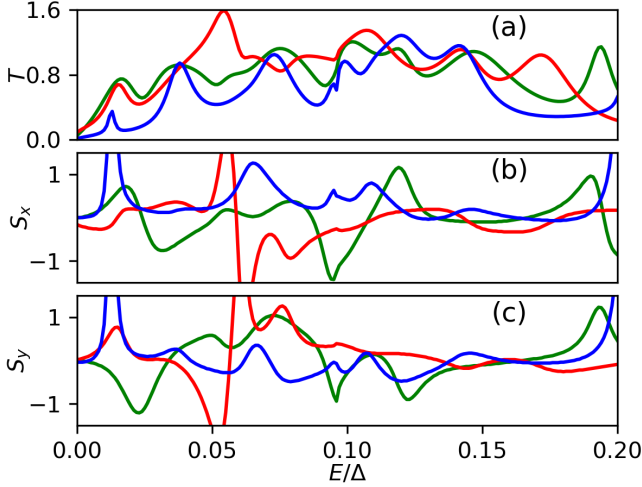

FIG. 3. Variation of (a) conductance (T) and spin response, (b) S_x, and (c)S_y function on 5th magnetic site.

classification algorithms, for e.g., Logistic regression [40], k-nearest neighbours (KNN) [41], Random Forest [42], Support Vector Machine (SVM) [43], etc. to train the models. Then, we use the trained models on the respective test samples and obtain the outputs. Among all the above classifiers the Random Forest performs the best and therefore we consider Random Forest throughout this paper. For comparison we also choose different regression models, for e.g., Theil-Sen regressor [44, 45], RANSAC (Random Sample Consensus) regressor [46], and SGD (Stochastic Gradient Descent) regressor [47] for the data analysis, but the regressors perform much worse than the classifiers.

Due to a rapid growth of the data size the training of modern machine learning systems is becoming a computationally intensive endeavour. The idea of using quantum computing in the field of machine learning is therefore becoming a highly desirable choice. One of the most popular quantum classifier is Quantum Support Vector Machine (QSVM) [48, 49], which is a quantized version classical SVM [43]. It performs the SVM algorithm using quantum computers. It calculates the kernel-matrix using the quantum algorithm for the inner product on quantum random access memory (QRAM) [50], and performs the classification of query data using the trained qubits with a quantum algorithm. The overall complexity of the quantum SVM is $\mathcal{O}\left(\log(NM)\right)$, whereas classical complexity of the SVM is $\mathcal{O}\left(M^2\left(M+N\right)\right)$, where N is the dimension of the feature space and M is the number of training vectors. The complexity of the Random forest (the best performing algorithm for our dataset) is $\mathcal{O}\left(TNMlogM\right)$, where M, N, and T are the number of instances in the training data, the number of attributes, and the number of trees respectively. Therefore, the QSVM model for the solution of classification and prediction offers upto exponential speed-up over its classical counterpart. Beside QSVM, an alternate class of quantum classification algorithm is introduced [51, 52], called Variational Quantum Classifier (VQC). This NISQ-friendly algorithm operates through using a variational quantum circuit to classify a training set in direct analogy to the conventional SVMs.

configuration. For simplicity we consider collinear magnetism ($\uparrow$ and $\downarrow$) while the energy is kept as a continuous variable. The formalism is also applicable for noncollinear magnetism, however it would expand the input parameter space since each magnetic moment has to be described by three components.

C. Classical and Quantum machine learning

Any machine learning approach consists of two steps - training and testing. For training one has to consider a large number of data where both inputs and outputs are known. For testing we use new input values and predict the output. For our case, we consider 17 input parameters . First 16 are the magnetisation direction of the 16 magnetic sites denoted by integers (1 for $\uparrow$ spin and 0 for $\downarrow$ spin) and the 17th input is the energy at which we calculate the desired output and is a floating number between 0.0 and 0.2. For output we consider conductance of the system and the x and y components of non-equilibrium spin density at each of the 16 magnetic sites. On each training sample we apply different

D. Regression vs classification

In previous works [31], the responses are considered in linear regime only where the regression techniques provide reasonable accuracy. However, for a highly nonlinear response, such as Fig. 3, applicability of regression becomes quite non-trivial. To increase the accuracy and efficiency of the learning process, here we adopt an alternative approach. First we discretise the output within small blocks and assign a class to each block (Fig. 4). To demonstrate that we consider the transmission spectrum corresponding to the green line in Fig. 3.

For a block height δ, the class of an output y is defined as $\mathcal{C}=\text{Round}[y/\delta]$, where Round[] represent rounding off
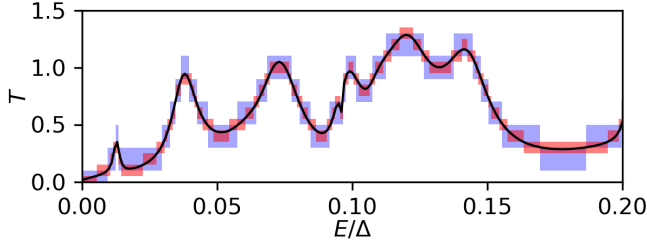
FIG. 4. Discretisation of the continuous output. Blue and red boxes correspond a block height of 0.2 and 0.1.

to the nearest integer. In this way a trained network can predict a class $\mathcal{C}$ for a unknown set of input parameters, from which one can retrieve the actual value y as $y = \mathcal{C}\delta$ and therefore δ correspond the intrinsic uncertainty of the discretisation. A larger value of δ would reduce the number of classes and therefore increase the accuracy of the prediction, however the predicted value can significantly differ from the actual value due to the uncertainty posed by δ and therefore increase the overall error. A small value of δ on the other hand can reduce the uncertainty, however it would increase the number of classes significantly and therefore may pose a computational challenge for the learning algorithm.

III. RESULTS AND DISCUSSIONS

As mentioned in Sec. II, we consider a scattering region with 16 magnetic site where the magnetisations can either point up or down. This gives a total of 2^{16} different configurations. For each of this configurations, one can calculate the transmission at any arbitrary energy which we choose between 0-0.2Δ. We are therefore dealing with a 17 dimensional feature space with mixed input variables where the first 16 inputs are either 0 (for spin $\downarrow$) or 1 (for spin $\uparrow$) and the 17th input is a floating number between 0 and 0.2 denoting the energy. For our study, we consider a set of 10^5 random input configurations and calculate corresponding transmission values and both the x and y component of spin response functions on all 16 magnetic sites. For classical machine learning algorithm the input parameters are the magnetic states of the 16 magnetic sites and the transport energy and the output is the transmission or the onsite spin response function.

A. Success rate vs accuracy with number of classes

The samples are randomly split into 9×10^4 training data and 10^4 testing data and then we conduct 50 different train-test cycles. The number of classes depends on the choice of the parameter δ. As discussed earlier, reducing δ can decrease the error, however it also increases the number of classes and therefore reduce the accuracy. Unless otherwise mentioned, we keep $\delta = 0.1$ which provides
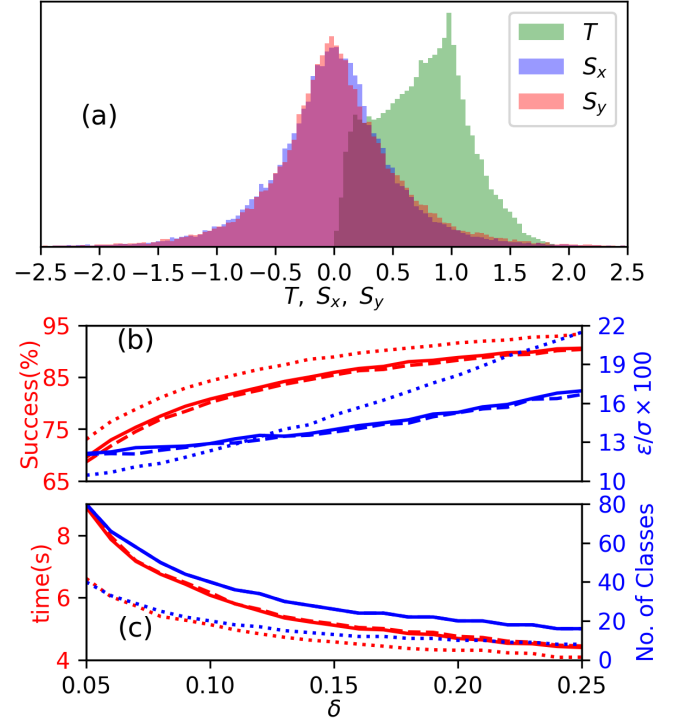

FIG. 5. Comparison of predictions for T, S_x, and S_y with respect to the discretisation parameter δ. (a) Distribution of the values of T, S_x, and S_y for $\delta = 0.1$. (b) Success rate of the prediction (red) and accuracy (ϵ/σ) (blue), where the the solid, dashed, and dotted lines correspond to S_x, S_y, and T respectively. (c) Time consumption (red) and number of classes (blue) for S_x (solid) and S_y (dashed) and T (dotted).

good balance between accuracy and error. Due to the highly non-linear nature of the system, there are few high values of the physical observable (Fig. 5a) which can significantly increase the total number of classes where the higher classes would have insignificant population. This is turns can reduce the performance of the learning algorithm. To avoid this scenario we put an upper cutoff of 2 for T and $S_{x,y}$, which means any value greater/less than ± 2 is considered as ± 2. The performance of prediction is characterised in terms of the success rate and accuracy which we define as the ratio of the root mean square error (RMSE) ϵ to the standard deviation of the output σ. This scales down the change of accuracy due to the variation of distribution of output classes. We try several training algorithms such as KNeighbors, DecisionTree and RandomForest. Among the methods Random forest shows better performance within reasonable execution time, and therefore we use Random forest throughout the rest of the study.

Note that unlike T, $S_{x,y}$ can have both positive and negative values and therefore for the same value of δ results in twice the number of classes for $S_{x,y}$ compared to T (Fig.5c). This enhancement of classes along with the localisation of spin density, as shown by the peaks in cause a slight reduction of success rate and detection

efficiency compared to that of T (Fig. 5b).

B. Prediction of transmission and spin response functions

As one can see from Fig. 2, the band structure and therefore the physical properties depend crucially on the choice of parameter. This in turns affects the distribution of the outputs and therefore the prediction itself. To demonstrate that we consider six different values of the parameter t_R, as showed in Fig. 2 and calculate 10^5 sample points by randomly varying the onsite magnetisation m_i and energy where the energy values are kept within $[0, 0.2\Delta]$. Training is done with randomly chose 9×10^4 data and the testing is done on rest of the 10^4 data points using Random forest algorithm. The accuracy and standard deviation is calculated by averaging over 50 different train-test cycles.

t_R/Δ	Success(%)	ϵ/σ	N_{class}	t_{Train}(s)	t_{Test}(s)
0.00	85.90	13.94	25	5.06	0.20
0.05	84.46	12.41	22	5.15	0.20
0.10	84.33	12.28	21	5.26	0.21
0.15	87.50	10.63	22	4.97	0.20
0.20	89.20	11.80	19	4.80	0.19
0.25	90.46	9.82	20	4.78	0.19

TABLE I. Qualitative variation of the prediction with respect to the Rashba parameter t_R.

From Table I, one can see that the quality of prediction gets better for higher value of t_R. This is because for smaller values of t_R, the entire energy range is not spanned by bands and therefore for a large number of input data the output remains 0. As we increase the value of t_R the selected energy range is covered with bands resulting more ordered finite output. For rest of the paper we consider $t_R=0.1\Delta$. To demonstrate the quality of the prediction we consider three configurations showed in Fig. 3a and evaluate the transmission coefficient on uniformly spaced energy values (Fig. 6a).

The spin response function is calculated via the onsite non-equilibrium spin expectation of the Pauli matrices. In our test system we have 16 magnetic centres where we calculate the spin response function. For this study we keep $t_R=0.1\Delta$ and train with Random forest algorithm. For brevity, we show S_x and S_y only at 6th magnetic site which has been showed for three specific configurations in Fig. 3.

To demonstrate the quality of our prediction we consider three particular configurations (Figs. 3b, 3c) and showed the predicted values against calculated values (Figs. 6b, 6c).
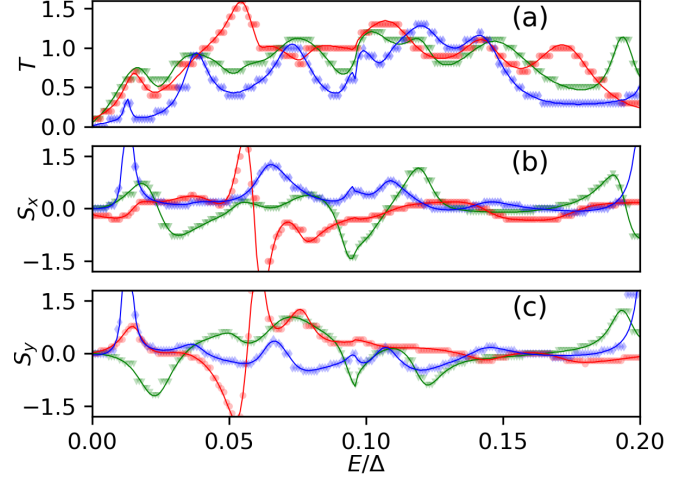

FIG. 6. Comparison of the predicted values against the actual values of (a) T, (b) S_x, and (c) S_y for three different configurations. The symbols show the predicted values and the lines show the numerically calculated values (Figs. 3b, 3c).

C. Application of quantum classifier

Finally we demonstrate the feasibility of quantum machine learning (QML) for our problem. Due to limitation of resources it is not possible to handle large number of input parameter or classes in this case. Therefore, we consider a particular magnetic configuration and choose the Rashba parameter (t_R) and the transmission energy (E) for the two components of the input variable and the sign of non-equilibrium $S_{x,y}$ on each site as the two output classes. We generate 1000 random input point in this two dimensional $t_R - E$ space and evaluate the sign of $S_{x,y}$ for each of the 16 magnetic sites. A sample dataset is presented in Fig. 7.
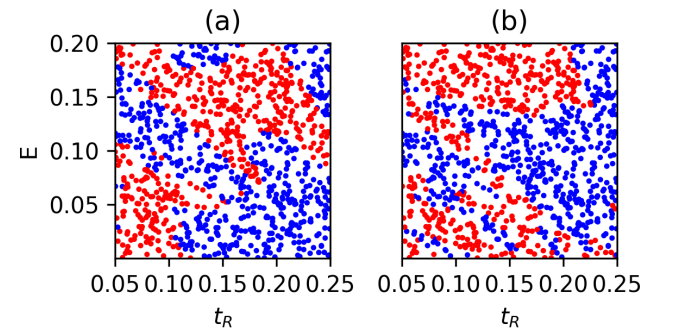

FIG. 7. A sample dataset with two features and two classes. Blue and red dots show the 0 and 1 classes for (a) S_x^6 and (b) S_y^6

We divide each dataset into two parts, namely, training data (900 data points) and testing data (100 data points). We implement classical SVM using Scikit-learn [53], and QSVM with Qiskit [54] from IBMQ, using different feature maps (for e.g., ZFeatureMap, ZZFeatureMap, etc.),

Quantity	QSVM	SVM(RBF)	SVM(Lin)	SVM(Poly)
S_x^1	83%	81%	58%	58%
S_y^1	78%	77%	71%	71%
S_x^2	83%	80%	79%	79%
S_y^2	90%	92%	93%	93%
S_x^3	77%	69%	54%	64%
S_y^3	79%	75%	62%	71%
S_x^4	85%	76%	71%	68%
S_y^5	82%	79%	82%	78%
S_x^5	82%	78%	73%	73%
S_y^5	84%	84%	51%	64%
S_x^6	83%	89%	64%	67%
S_y^6	76%	75%	63%	69%
S_x^7	75%	75%	58%	70%
S_y^7	80%	73%	63%	70%
S_x^8	78%	81%	66%	68%
S_y^8	74%	75%	60%	64%

TABLE II. Comparing the testing accuracies between different classical and quantum classifiers for the S_x and S_y for first 8 magnetic sites. In the above table RBF, Lin, and Poly represents the RBF, Linear, and Polynomial Kernels used in SVM algorithm.

to classify the data. We repeat the above procedure with all the 16 datasets and summarize the result in table II. For brevity we show $S_{x,y}$ for only first 8 sites.

From table II, we see that the quantum classifier is performing better than it's classical counterparts in many cases. Although, the main advantage of QML over classical ML is in the runtime (see Sec. II C), so that, for a significantly larger data size and configuration space QML will be the only feasible option. Therefore, with the availability of sufficient quantum computing resources this approach will be very useful to analyse the large solid state and molecular devices as well.

IV. CONCLUSION

In this article, we demonstrate the applicability of different classical and quantum machine learning approachs for spintronics. We show that how one can achieve a significantly improved performance by converting the conventional regression problem into a discretised classification problem. Our approach allows us to obtain a high level of accuracy even for a strongly nonlinear regime. We further demonstrate the applicability of quantum machine learning which performs quite well for our small feature space. Considering the scalability of quantum machine learning algorithms over their classical counter parts (see Sec. II C) this will significantly enhance the performance for a larger configuration space and data size; in fact QML will be the only viable option in that regime. Although we consider a standard magnetic configuration considering a solid state device, this method is equally applicable for a large class of systems, especially, the molecular devices where one can easily use charge or orbital degrees of freedom along with the spin to control different physical observables. Our work thus opens new possibilities to study a large variety of physical system and their physical properties with machine learning.

[1] S. Russell, P. Norvig, and J. Canny, *Artificial Intelligence: A Modern Approach*, Prentice Hall series in artificial intelligence (Prentice Hall/Pearson Education, 2003).

[2] M. A. Nielsen and I. Chuang, Quantum computation and quantum information (2002).

[3] N. Artrith, K. T. Butler, F.-X. Coudert, S. Han, O. Isayev, A. Jain, and A. Walsh, Nat. Chem. **13**, 505 (2021).

[4] K. T. Schütt, M. Gastegger, A. Tkatchenko, K.-R. Müller, and R. J. Maurer, Nat. Commun. **10**, 1 (2019).

[5] J. P. Janet and H. J. Kulik, *Machine Learning in Chemistry* (American Chemical Society, 2020).

[6] C. Pang, F. Prabhakara, A. El-abiad, and A. Koivo, IEEE Transactions on Power Apparatus and Systems **PAS-93**, 969 (1974).

[7] H. Ghoddusi, G. G. Creamer, and N. Rafizadeh, Energy Economics **81**, 709 (2019).

[8] Y. Xin, L. Kong, Z. Liu, Y. Chen, Y. Li, H. Zhu, M. Gao, H. Hou, and C. Wang, IEEE Access **6**, 35365 (2018).

[9] S. Omar, A. Ngadi, and H. H. Jebur, International Journal of Computer Applications **79**, 33 (2013).

[10] J. Vamathevan, D. Clark, P. Czodrowski, I. Dunham, E. Ferran, G. Lee, B. Li, A. Madabhushi, P. Shah, M. Spitzer, and S. Zhao, Nat. Rev. Drug Discov. **18**, 463 (2019).

[11] J. Preskill, Quantum **2**, 79 (2018).

[12] M. Schuld, I. Sinayskiy, and F. Petruccione, Contemporary Physics **56**, 172 (2014).

[13] J. Biamonte, P. Wittek, N. Pancotti, P. Rebentrost, N. Wiebe, and S. Lloyd, Nature **549**, 195 (2017).

[14] A. Sakhnenko, C. O'Meara, K. Ghosh, C. B. Mendl, G. Cortiana, and J. Bernabé-Moreno, arXiv:2112.08869 [quant-ph] 10.48550/arXiv.2112.08869 (2021).

[15] S. Woerner and D. J. Egger, npj Quantum Inf. **5**, 1 (2019).

[16] B. P. Lanyon, J. D. Whitfield, G. G. Gillett, M. E. Goggin, M. P. Almeida, I. Kassal, J. D. Biamonte, M. Mohseni, B. J. Powell, M. Barbieri, A. Aspuru-Guzik, and A. G. White, Nat. Chem. **2**, 106 (2010).

[17] Y. Cao, J. Romero, J. P. Olson, *et al.*, Chem. Rev. **119**, 10856 (2019).

[18] A. Kandala, A. Mezzacapo, K. Temme, M. Takita, M. Brink, J. M. Chow, and J. M. Gambetta, Nature **549**, 242 (2017).

[19] R. Eskandarpour, K. Ghosh, A. Khodaei, A. Paaso, and L. Zhang, IEEE Access **8**, 188993 (2020).

[20] R. Eskandarpour, K. Ghosh, A. Khodaei, and A. Paaso, arXiv:2106.12032 [quant-ph] 10.48550/arXiv.2106.12032 (2021).

[21] V. Giovannetti, S. Lloyd, and L. Maccone, Science **306**, 1330 (2004).

[22] A. Wichert, *Principles of quantum artificial intelligence: quantum problem solving and machine learning* (World Scientific, 2020).

[23] E. Bedolla, L. C. Padierna, and R. Castañeda-Priego, J. Phys.: Condens. Matter **33**, 053001 (2020).

[24] R. Xia and S. Kais, Nat. Commun. **9**, 1 (2018).

[25] J. Weber, W. Koehl, J. Varley, A. Janotti, B. Buckley, C. Van de Walle, and D. D. Awschalom, PNAS **107**, 8513 (2010).

[26] A. Smith, M. Kim, F. Pollmann, and J. Knolle, npj Quantum Inf **5**, 1 (2019).

[27] A. Chandrasekaran, D. Kamal, R. Batra, C. Kim, L. Chen, and R. Ramprasad, npj Comput Mater **5**, 1 (2019).

[28] J. Westermayr, M. Gastegger, K. T. Schütt, and R. J. Maurer, J. Chem. Phys. **154**, 230903 (2021), arXiv:2102.08435.

[29] L. Fiedler, K. Shah, M. Bussmann, and A. Cangi, Phys. Rev. Materials **6**, 040301 (2022).

[30] A. Lopez-Bezanilla and O. A. von Lilienfeld, Phys. Rev. B **89**, 235411 (2014), arXiv:1401.8277.

[31] T. Wu and J. Guo, IEEE Trans. Electron Devices **67**, 5229 (2020).

[32] A. Manchon and S. Zhang, Phys. Rev. B **78**, 212405 (2008).

[33] A. Manchon and S. Zhang, Phys. Rev. B **79**, 094422 (2009).

[34] S. Ghosh and A. Manchon, Phys. Rev. B **95**, 035422 (2017), arXiv:1609.01174.

[35] S. Ghosh and A. Manchon, Phys. Rev. B **97**, 134402 (2018), arXiv:1711.11016.

[36] S. Ghosh and A. Manchon, Phys. Rev. B **100**, 014412 (2019), arXiv:1901.08314.

[37] B. K. Nikolić, S. Souma, L. P. Zârbo, and J. Sinova, Phys. Rev. Lett. **95**, 046601 (2005).

[38] B. K. Nikolić, K. Dolui, M. D. Petrović, P. Plecháč, T. Markussen, and K. Stokbro, in *Handb. Mater. Model.* (Springer International Publishing, 2018) pp. 1–35, arXiv:1801.05793.

[39] C. W. Groth, M. Wimmer, A. R. Akhmerov, and X. Waintal, New J. Phys. **16**, 063065 (2014), arXiv:1309.2926.

[40] D. G. Kleinbaum and M. Klein, *Logistic regression* (Springer, 2002).

[41] O. Kramer, K-nearest neighbors, in *Dimensionality Reduction with Unsupervised Nearest Neighbors* (Springer Berlin Heidelberg, Berlin, Heidelberg, 2013) pp. 13–23.

[42] L. Breiman, Machine learning **45**, 5 (2001).

[43] C. Cortes and V. Vapnik, Machine learning **20**, 273 (1995).

[44] H. Theil, Indagationes mathematicae **12**, 173 (1950).

[45] P. K. Sen, Journal of the American Statistical Association **63**, 1379 (1968).

[46] M. A. Fischler and R. C. Bolles, Communications of the ACM **24**, 381 (1981).

[47] L. Bottou and O. Bousquet, in *Advances in Neural Information Processing Systems*, Vol. 20, edited by J. Platt, D. Koller, Y. Singer, and S. Roweis (Curran Associates, Inc., 2007).

[48] J. Pan, Y. Cao, X. Yao, Z. Li, C. Ju, H. Chen, X. Peng, S. Kais, and J. Du, Phys. Rev. A **89**, 022313 (2014).

[49] Z. Li, X. Liu, N. Xu, and J. Du, Phys. Rev. Lett. **114**, 140504 (2015).

[50] V. Giovannetti, S. Lloyd, and L. Maccone, Phys. Rev. Lett. **100**, 160501 (2008).

[51] K. Mitarai, M. Negoro, M. Kitagawa, and K. Fujii, Phys. Rev. A **98**, 032309 (2018).

[52] V. Havlíček, A. D. Córcoles, K. Temme, A. W. Harrow, A. Kandala, J. M. Chow, and J. M. Gambetta, Nature **567**, 209 (2019).

[53] F. Pedregosa, G. Varoquaux, A. Gramfort, V. Michel, B. Thirion, O. Grisel, M. Blondel, P. Prettenhofer, R. Weiss, V. Dubourg, *et al.*, the Journal of machine Learning research **12**, 2825 (2011).

[54] G. Aleksandrowicz *et al.*, Qiskit: An open-source framework for quantum computing (2021).